Publisher: GSA
Journal: GEOL: Geology
DOI:10.1130/G36677.1

Duration and dynamics of the best orbital analogue to the present interglacial

Biagio Giaccio[1]*, Eleonora Regattieri[1,2,3], Giovanni Zanchetta[1,2,3], Sebastien Nomade[4], Paul R. Renne[5,6], Courtney J. Sprain[5,6], Russell N. Drysdale[7,8], Polychronis C. Tzedakis[9], Paolo Messina[1], Giancarlo Scardia[1,10], Andrea Sposato[1], and Franck Bassinot[5]

[1]*CNR-Istituto di Geologia Ambientale e Geoingegneria, Via Salaria km 29,300, 00015 Monterotondo, Rome, Italy*

[2]*Dipartimento di Scienze della Terra, Università di Pisa, Via S. Maria 53, 56126 Pisa, Italy*

[3]*Istituto di Geoscienze e Georisorisorse IGG-CNR, Italy, Via Giuseppe Moruzzi 1, 56124 Pisa, Italy*

[4]*Laboratoire des Sciences du Climat et de l'Environnement (CEA-CNRS-UVSQ), Avenue de la terrasse, Bât 12 91198 Gif Sur Yvette cedex, France*

[5]*Berkeley Geochronology Center, 2455 Ridge Road, Berkeley, California 94709, USA*

[6]*Department of Earth and Planetary Science, University of California–Berkeley, Berkeley, California 94720, USA*

[7]*School of Geography, The University of Melbourne, 221 Bouverie Street, Carlton, 3052 Victoria, Australia*

[8]*Laboratoire EDYTEM, Université de Savoie, Pôle Montagne, 73376 Le Bourget du Lac cedex, France*

Publisher: GSA
Journal: GEOL: Geology
DOI:10.1130/G36677.1
[9]*Department of Geography, University College London, Pearson Building, Gower Street, London WC1E 6BT, UK*

[10]*Instituto de Geociências e Ciências Exatas, Universidade Estadual Paulista, Rio Claro, SP 13506-900, Brazil*

*E-mail: biagio.giaccio@cnr.it

ABSTRACT

Past orbital analogues to the present interglacial, such as Marine Isotope Stage 19c (MIS 19c, ca. 800 ka), can provide reliable reference intervals for evaluating the timing and the duration of the Holocene and factors inherent its climatic progression. Here we present the first high-resolution palaeoclimatic record for MIS 19 anchored to a high-precision $^{40}Ar/^{39}Ar$ chronology, thus, fully independent from any a priori assumptions on the orbital mechanisms underlying the climatic changes. It is based on the oxygen isotope compositions of Italian lake sediments showing orbital to millennial-scale hydrological variability over the Mediterranean between 810 ka and 750 ka. Our record indicates that the MIS 19c interglacial lasted 10.8 ± 3.7 k.y.—comparable to the time elapsed since onset of the Holocene—and that the orbital configuration at the time of the following glacial inception was very similar to the present one. By analogy, the current interglacial should be close to its end. However, greenhouse gas concentrations at the time of the MIS 19 glacial inception were significantly lower than those of the late Holocene, suggesting that the current interglacial could have already been prolonged by the progressive increase of the greenhouse gases since 8–6 ka, possible due to early anthropogenic disturbance of vegetation.

INTRODUCTION

Publisher: GSA
Journal: GEOL: Geology
DOI:10.1130/G36677.1

The Milankovitch paradigm for the response of Earth's climatic system to astronomical forcing provides the theoretical framework to explain the pacing of interglacial-glacial cycles (Hays et al., 1976). It predicts that the onset of interglacials occurs close to the boreal summer insolation maximum/precession minimum, but glacial inceptions defy the theoretical prediction because they lack a systematic relation to insolation (Tzedakis et al., 2012a). Furthermore, although climate models have demonstrated how the reduction in boreal summer insolation plays a predominant role for glacial inception (Calov et al., 2009), uncertainty regarding the timing of the next glacial onset still persists because of the low orbital eccentricity that will characterize the next 100 k.y., which results in a very subdued amplitude of insolation variability (e.g., Loutre and Berger, 2000).

The study of the past interglacial analogs for the Holocene, or Marine Isotope Stage 1 (MIS 1), may thus be pivotal for evaluating the temporal extent of the present interglacial. Although not perfectly identical to MIS 1, in terms of orbital configuration, insolation distribution pattern and temperature response, MIS 19 can be considered the closest to the current interglacial (e.g., Yin and Berger, 2012). The MIS 19 interglacial (MIS 19c) is well expressed in marine (Channell et al., 2010) and ice (Jouzel et al., 2007) records. However, the age models of these records are entirely or partially dependent upon astrochronology, and thus the recent estimation of ~12.5 k.y. for the duration of MIS 19c (Tzedakis et al., 2012b) rests on the assumed validity of the orbital tuning approach. In order to address this issue independent of any a priori assumptions, we assembled the first high-precision $^{40}Ar/^{39}Ar$ dated high-resolution palaeoclimatic record for this interval from Italian lacustrine sediments (Fig. 1), which preserve a history of

Publisher: GSA
Journal: GEOL: Geology
DOI:10.1130/G36677.1
hydrological variability and temporal progression of the MIS 19c in the Mediterranean area.

METHODS AND RESULTS

Stratigraphy and Lithology of the Investigated Sulmona 6 Unit

Our study focused on the ~30-m-thick basal interval (20–50 m depth) of the Sulmona 6 (SUL6) lacustrine unit (central Apennine, Italy; Fig. 1), spanning the ca. 820–720 ka interval and encompassing the Matuyama-Brunhes geomagnetic reversal (Giaccio et al., 2013; Sagnotti et al., 2014). With the exception of a meter-thick peaty layer in the upper portion of the succession (at ~26 m depth, Fig. 1), lithology consists of whitish massive to faintly laminate marls that indicate a continuous sedimentation in a relatively deep lake environment. X-ray diffraction and scanning electron microscope analyses reveal that the non-clay fraction of the lacustrine sediments from unit SUL6 is mainly composed of euhedral to subhedral calcite crystals of ~10–15 μm, typical of biogenic precipitation (e.g., Kelts and Hsü, 1978).

Proxy Data and Their Palaeoclimatic Interpretation

Both oxygen isotope ratios ($\delta^{18}O$) and percent $CaCO_3$ depth series from SUL6 unit (Fig. DR1 and methods in the GSA Data Repository[1]) show notable variations that reflect changes in hydrological regime. The $\delta^{18}O$ of carbonates from Mediterranean lakes and caves (speleothems) is an established proxy for regional hydrological variability, which is modulated by the proportion of advected air masses from the North Atlantic to the basin, and thus an indirect expression of the boreal subpolar climate variability (e.g., Roberts et al., 2008).

Publisher: GSA
Journal: GEOL: Geology
DOI:10.1130/G36677.1

The content of $CaCO_3$ is related to lake bioproductivity, which is low under glacial/stadial climatic conditions, during which the proportion of siliciclastic sedimentary input from rivers is higher, and high during interglacial/interstadial periods (Vogel et al., 2010). This is also reflected in the measurements of sediment magnetic susceptibility which varies as the complement to the carbonate content (Fig. DR1).

Chronology

We refined the previous chronology of the SUL6 unit (Giaccio et al., 2013; Sagnotti et al., 2014) by six additional, high-precision $^{40}Ar/^{39}Ar$ dates, which yielded 13 ages for seven different tephras, with small analytical uncertainties of 2–3‰ (Fig. 1; Table DR1). Specifically, the ages from five of these tephras were determined by combining the results from paired subsamples dated in two different laboratories—Berkeley Geochronology Center (Berkley, California, USA) and CNRS Le Laboratoire des Sciences du Climat et de l'Environnement (Gif Sur Yvette, France)—each yielding statistically indistinguishable ages (Table DR1; Fig. DR2; full analytical details are given in Data sets DR1 and DR2).

The final Bayesian depth-age model was based upon the six age-control points below the peat layer at ~26 m depth (Table DR1), which marks a lake-level low-stand and possibly a sedimentation hiatus (Fig. 1). The resulting record spans ~805–750 k.y., with a temporal resolution of 100–200 yr for the $\delta^{18}O$ time series (Fig. 1).

DISCUSSION

The MIS 19 isotope record for Sulmona reproduces in detail the variability observed in the reference records of the European Project for Ice Coring in Antarctica (EPICA) Dome C Antarctic ice (Jouzel et al., 2007) and of planktonic $\delta^{18}O$ from the

Publisher: GSA
Journal: GEOL: Geology
DOI:10.1130/G36677.1
subpolar North Atlantic Ocean Drilling Progam (ODP) Site 983 (Channell et al., 2010), including a series of abrupt, millennial-scale oscillations (Fig. 2). In contrast with these reference records, the Sulmona succession has the advantage of yielding precise ages for estimating the duration of the MIS 19c, independent of any orbital assumptions. Indeed, although several calibrations are in use for the $^{40}Ar/^{39}Ar$ method, which yield absolute ages that vary by ~2% in the Pleistocene (e.g., Sagnotti et al., 2014), the chronological resolution of the method, i.e., relative $^{40}Ar/^{39}Ar$ age, is unaffected by uncertainties in absolute calibration and is limited only by analytical precision (~2–3‰; Fig. DR2). Furthermore, the Sulmona record also provides indirect but closely related proxy evidence of the North Atlantic millennial-scale variability, which is a key feature for defining interglacial/glacial boundaries (Tzedakis et al., 2012a).

While the formal distinction between glacials and interglacials is mostly related to ice volume/ sea level, an indirect indication of the growth of the ice sheets is provided by millennial-scale records of ice-rafted debris (IRD) produced by iceberg discharges to the North Atlantic, which trigger Northern Hemisphere cold events and bipolar seesaw oscillations (Tzedakis et al., 2012a). These cold events can be traced in Mediterranean marine and terrestrial records as sea-surface cooling (e.g., Martrat et al., 2014) and decreases in precipitation, as revealed by pollen (e.g., Brauer et al., 2007) and lake/speleothem $\delta^{18}O$ (e.g., Regattieri et al., 2015) records. Both direct and indirect IRD proxy records provide, however, a late indication of glacial inception, because the first IRD events that follow the interglacials occur only once the ice sheets extend to coastlines and reach the critical size for collapsing, i.e., some millennia after the onset of the ice growth (Tzedakis et al., 2012a). A less ambiguous definition of interglacial onset,

Publisher: GSA
Journal: GEOL: Geology
DOI:10.1130/G36677.1
analogous to the Holocene (Walker et al., 2012), can be identified from the end of the terminal bipolar seesaw oscillation, or Younger Dryas (YD)–like cold/dry event, of the preceding glacial periods, which is a pervasive feature of the last nine glacial-interglacial transitions (Broecker et al., 2010; Barker et al., 2011). This notion of interglacial boundaries could differ from the formal one based on ice volume/ sea level. Nevertheless it provides unambiguous stratigraphic criteria for delimiting intervals that approach the length of the sea-level highstands and for consistently comparing different interglacials, which is the purpose of the present paper.

Full interglacial conditions in the Sulmona isotope record occur sharply at the end of the last, YD-like drier pulse dated at 790.6 ± 2.5 ka (95%-confidence), which interrupts the preceding long-term wetting-trend started at ca. 805 ka (Figs. 2G and 3E). Following an ~8-k.y.-long period of relative stability, the Sulmona MIS 19 record shows a progressive, ~7-k.y.-long, trend of isotope enrichment, which culminates in the first marked dry episode that can be correlated with the earliest IRD event in North Atlantic, and thus to the re-establishment of the millennial-scale bipolar seesaw (Fig. 2G). From the above theoretical considerations, the end of MIS 19c should consequently fall within this millennial-long drying trend of the Sulmona record that would represent the local hydrological response to ice sheet growth (Fig. 3E). Conceivably, it could thus coincide with the definitive increase of $\delta^{18}O$ beyond the value of ~– 8.4 ‰ at 779.8 ± 2.8 ka, which corresponds to the maximum threshold reached by the minor $\delta^{18}O$ excursions during the period of unambiguous interglacial condition (Fig. 3E). The total duration of the Sulmona MIS 19c derived from our age model is 10.8 ± 3.7 k.y. (2σ; Fig. 3). This duration is robust across other age models, including simple piecewise linear

Publisher: GSA
Journal: GEOL: Geology
DOI:10.1130/G36677.1
interpolation of age-depth data, which yields a duration of 11.6 ± 2.3 k.y. Although our preferred duration estimate might statistically extend up to ~14.5–13.5 k.y. (~4% probability), there is a higher probability that it is within ~12.5–9.0 k.y. (~68%), and thus to approach the astrochronological estimation of the MIS 19c length (~12.5 k.y.; Tzedakis et al., 2012b) as well as the time elapsed since the inception of the Holocene (Fig. 3D).

In order to compare MIS 19 and MIS 1, we synchronized the Sulmona MIS 20-MIS 19 and the Late Glacial-Holocene sea surface palaeotemperature record from Alboran Sea (Martrat et al., 2014), anchored to the respective orbital parameters, along the abrupt end of the YD-like oscillation, which is clearly documented at the glacial-interglacial transition of both series (Figs. 3D and 3E). In spite of the large uncertainty for the absolute ages of the MIS 19c boundaries, this alignment shows that the overall astronomical configuration for the start and end of MIS 19c is in good agreement with the Milankovitch pacing of the MIS 20-MIS 19 glacial-interglacial transition and replicates the Holocene configuration quite well (Figs. 3A–3C). Substantial coherence between the two palaeoclimatic time periods is also evident, particularly the long-term cooling trend and the minor oscillations in the Alboran Sea record have similar hydrological expressions in the Sulmona MIS 19c record (Figs. 3D and 3E). Consequently, by analogy between MIS 19c and MIS 1, the current interglacial should be very close to its end. However, when considering the others relevant factor required for triggering a glacial inception, i.e., the atmospheric greenhouse gas concentrations (e.g,. CO_2), a substantial difference between the MIS 19 and MIS 1 emerges. At the time of the MIS 19 glacial inception, the corresponding CO_2 content in EPICA Dome C ice was ~250 ppm (Bereiter

Publisher: GSA
Journal: GEOL: Geology
DOI:10.1130/G36677.1
et al., 2015; Fig. 3G), while the preindustrial concentration of CO_2 was ~280 ppm, and over the entire Holocene it never fell below ~260 ppm, which was reached at ca. 8–6 ka (Monnin et al., 2004; Fig. 3G). On the other hand, according to the Early Anthropogenic Hypothesis (Ruddiman, 2007), in the absence of early agricultural greenhouse gas emissions, the late Holocene CO_2 levels should have fallen to ~245 ppm, i.e., close to the value observed near the end of MIS 19c. The case of delayed or failed glaciation caused by the progressive, possibly anthropogenic, increase of atmospheric CO_2 concentrations since ca. 8–6 ka would seem to be supported by the results of the present study.

CONCLUDING REMARKS

The Sulmona record provides the first independent radioisotopic validation of the astrochronological time scales of ice-core and marine records for the MIS 19c and thus of the previous estimation of its length deduced from these time series.

The MIS 19c-MIS 1 comparison suggests that the variability and the total duration of MIS 19c interglacial in our record (10.8 ± 3.7 k.y., 2σ) are comparable to those of the elapsed period since onset of the current interglacial (ca. 11.7 ka) and that the astronomical configuration required for driving the MIS 1 glacial inception should have already been reached. However, the expected shifting of the late Holocene climate system into a glacial period might have been delayed or inhibited by the relatively higher levels of the CO_2 concentration. Regardless of the remaining uncertainty on the causes underlying the difference in greenhouse gas levels during the MIS 19 and the preindustrial-Holocene (i.e., Early Anthropogenic Hypothesis versus “natural”), this would have been enough to drastically deviate the evolutionary climatic trajectories of

the two orbital analogs interglacials, highlighting a very high sensitivity of the climate to greenhouse gases.

ACKNOWLEDGMENTS

We thank Valerie Masson-Delmotte for her critical review of an early manuscript. The paper also benefited from insightful comments from Bill Ruddiman and five anonymous reviewers. Regattieri is supported by a Ph.D. grant of the School of Graduate Studies Galileo Galilei (University of Pisa, Italy). $^{40}Ar/^{39}Ar$ ages were supported by the Ann and Gordon Getty Foundation (BGC), and by a SYSTER National Institute for Earth Sciences and Astronomy 2013 program (Gif). Tzedakis acknowledges funding from the Natural Environment Research Council (grant NE/I025115/1). Giaccio thanks La Locanda di Gino in Sulmona, Italy, for valuable help in the field.

REFERENCES CITED

Barker, S., Knorr, G., Lawrence Edwards, R., Parrenin, F., Putnam, A.E., Skinner, L.C., Wolff, E., and Ziegler, M., 2011, 800,000 years of abrupt climate variability: Science, v. 334, p. 347–351, doi:10.1126/science.1203580.

Bazin, L., et al., 2013, An optimized multi-proxy, multi-site Antarctic ice and gas orbital chronology (AICC2012): 120–800 ka: Climate of the Past, v. 9, p. 1715–1731, doi:10.5194/cp-9-1715-2013.

Berger, A., and Loutre, M.F., 1991, Insolation values for the climate of the last 10 million years: Quaternary Science Reviews, v. 10, p. 297–317, doi:10.1016/0277-3791(91)90033-Q.

Blaauw, M., and Christen, J.A., 2011, Flexible paleoclimate age-depth models using an autoregressive gamma process: Bayesian Analysis, v. 6, p. 457–474, doi:10.1214/ba/1339616472.

Brauer, A., Allen, J.R.M., Mingram, J., Dulski, P., Wulf, S., and Huntley, B., 2007, Evidence for the last interglacial chronology and environmental change from Southern Europe: Proceedings of the National Academy of Sciences of the United States of America, v. 104, p. 450–455, doi:10.1073/pnas.0603321104.

Bereiter, B., Eggleston, S., Schmitt, J., Nehrbass-Ahles, C., Stocker, T.F., Fischer, H., Kipfstuhl, S., and Chappellaz, J., 2015, Revision of the EPICA Dome C CO2 record from 800 to 600 kyr before present: Geophysical Research Letters, v. 42, no. 2, p. 542–549, doi:10.1002/2014GL061957.

Broecker, W.S., Denton, G.H., Edwards, R.L., Cheng, H., Richard, B., Alley, R.B., and Putnam, A.E., 2010, Putting the Younger Dryas cold event into context: Quaternary Science Reviews, v. 29, p. 1078–1081, doi:10.1016/j.quascirev.2010.02.019.

Calov, R., Ganopolski, A., Kubatzki, C., and Claussen, M., 2009, Mechanisms and time scales of glacial inception simulated with an Earth system model of intermediate complexity: Climate of the Past, v. 5, p. 245–258, doi:10.5194/cp-5-245-2009.

Channell, J.E.T., Hodell, D.A., Singer, B.S., and Xuan, C., 2010, Reconciling astrochronological and 40Ar/39Ar ages for the Matuyama-Brunhes boundary and late Matuyama Chron: Geochemistry Geophysics Geosystems, v. 11, Q0AA12, doi: 10.1029/2010GC003203.

EPICA (European Project for Ice Coring in Antarctica) community members, 2006, One-to-one coupling of glacial climate variability in Greenland and Antarctica: Nature, v. 195–198, doi:10.1038/nature05301.

Giaccio, B., Castorina, F., Nomade, S., Scardia, G., Voltaggio, M., and Sagnotti, L., 2013, Revised chronology of the Sulmona lacustrine succession, central Italy: Journal of Quaternary Science, v. 28, p. 545–551, doi:10.1002/jqs.2647.

Hays, J.D., Imbrie, J., and Shackleton, N.J., 1976, Variations in the Earth's orbit: pacemaker of the ice ages: Science, v. 194, p. 1121–1132, doi:10.1126/science.194.4270.1121.

Jouzel, J., et al., 2007, Orbital and millennial Antarctic climate variability over the past 800,000 years: Science, v. 317, p. 793–796, doi:10.1126/science.1141038.

Kelts, K., and Hsü, K.J., 1978, Freshwater carbonate sedimentation, *in* Lerman, A., ed., Lakes, Chemistry, Geology, Physics: Berlin, Springer-Verlag, p. 295–323.

Kleiven, H.F., Hall, I.R., McCave, I.N., Knorr, G., and Jansen, E., 2011, Coupled deep-water flow and climate variability in the middle Pleistocene North: Atlantic Geology, v. 39, p. 343–346, doi:10.1130/G31651.1.

Loulergue, L., Schilt, A., Spahni, R., Masson-Delmotte, V., Blunier, T., Lemieux, B., Barnola, J.-M., Raynaud, D., Stocker, T.F., and Chappellaz, J., 2008, Orbital and millennial-scale features of atmospheric CH_4 over the past 800,000 years: Nature, v. 453, p. 383–386, doi:10.1038/nature06950.

Loutre, M.F., and Berger, A., 2000, Future climatic changes: are we entering an exceptionally long interglacial?: Climatic Change, v. 46, p. 61–90, doi:10.1023/A:1005559827189.

Martrat, B., Jimenez-Amat, P., Zahn, R., and Grimalt, J.O., 2014, Similarities and dissimilarities between the last two deglaciations and interglaciations in the North Atlantic region: Quaternary Science Reviews, v. 99, p. 122–134, doi:10.1016/j.quascirev.2014.06.016.

Monnin, E., et al., 2004, Evidence for substantial accumulation rate variability in Antarctica during the Holocene, through synchronization of CO_2 in the Taylor Dome, Dome C and DML ice cores: Earth and Planetary Science Letters, v. 224, p. 45–54, doi:10.1016/j.epsl.2004.05.007.

Regattieri, E., Giaccio, B., Zanchetta, G., Drysdale, R.S., Galli, P., Peronace, E., Nomade, S., and Wulf, S., 2015, Hydrological variability over Apennine during the Early Last Glacial precession minimum, as revealed by a stable isotope record from Sulmona basin, central Italy: Journal of Quaternary Science, v. 30, p. 19–31, doi:10.1002/jqs.2755.

Roberts, N., et al., 2008, Stable isotope records of Late Quaternary climate and hydrology from Mediterranean lakes: The ISOMED synthesis: Quaternary Science Reviews, v. 27, p. 2426–2441, doi:10.1016/j.quascirev.2008.09.005.

Ruddiman, W.F., 2007, The early anthropogenic hypothesis: Challenges and responses: Reviews of Geophysics, v. 45, p. RG4001, doi:10.1029/2006RG000207.

Sagnotti, L., Scardia, G., Giaccio, B., Liddicoat, J.C., Nomade, S., Renne, P.R., and Sprain, C.J., 2014, Extremely rapid directional change during Matuyama-Brunhes geomagnetic polarity reversal: Geophysical Journal International, v. 199, p. 1110–1124, doi:10.1093/gji/ggu287.

Tzedakis, P.C., Wolff, E.W., Skinner, L.C., Brovkin, V., Hodell, D.A., McManus, J.F., and Raynaud, D., 2012a, Can we predict the duration of an interglacial?: Climate of the Past, v. 8, p. 1473–1485, doi:10.5194/cp-8-1473-2012.

Tzedakis, P.C., Channell, J.E.T., Hodell, D.A., Kleiven, H.F., and Skinner, L.C., 2012b, Determining the natural length of the current interglacial: Nature Geoscience, v. 5, p. 138–141, doi:10.1038/ngeo1358.

Vogel, H., Zanchetta, G., Sulpizio, R., Wagner, B., and Nowaczyk, N.A., 2010, Tephrostratigraphic record for the last glacial-interglacial cycle from Lake Ohrid, Albania and Macedonia: Journal of Quaternary Science, v. 25, p. 320–338, doi:10.1002/jqs.1311.

Walker, M.J.C., et al., 2012, Formal subdivision of the Holocene Series/Epoch: a Discussion Paper by a Working Group of INTIMATE (Integration of ice-Core, Marine and Terrestrial Records) and the Subcommission on Quaternary Stratigraphy (International Commission on Stratigraphy): Journal of Quaternary Science, v. 27, p. 649–659, doi: 10.1002/jqs.2565.

Yin, Q.Z., and Berger, A., 2012, Individual contribution of insolation and CO_2 to the interglacial climates of the past 800,000 years: Climate Dynamics, v. 38, p. 709–724, doi:10.1007/s00382-011-1013-5.

FIGURE CAPTIONS

Figure 1. Bayesian age model for the 30-m-thick basal interval of the composite core-outcrop Sulmona 6 (SUL6) unit (central Apennine, Italy; Giaccio et al., 2013). For comparison, the outcrop depth is also shown. The depth-age model (thin black line) and corresponding 95% confidence limits (thick gray line) are based on Bacon software

Publisher: GSA
Journal: GEOL: Geology
DOI:10.1130/G36677.1
(Blaauw and Christen, 2011) applied to $^{40}Ar/^{39}Ar$ dating and corresponding 95% confidence uncertainties (white dots and related error bars, tapered horizontal bars represent the full propagated errors as generated by Bacon software), from both present and previous studies (Table DR1 [see footnote 1]). The Marine Isotope Stage 19c (MIS 19c) interglacial is recorded in the ~4-m-thick highlighted interval between the depths of ~38.6 m and ~42.7 m. The resulting sedimentation rate (Sed. rate) and temporal resolution for the oxygen isotope record (Resolution) are also shown. Dashed line represents the interval with uncertain sedimentation rate—not considered for the final age model and proxy records—which includes the lake-level low stand-related peat layer just above the SUL2–7 tephra. Inset, location of the Sulmona basin (42°09′14”N, 13°49′05”E).

Figure 2. Palaeoclimatic records and orbital parameters for the Marine Isotope Stage (MIS) 20–MIS 18 period. A: Marine Isotope stages. B–D: 21 June insolation at 65°N, precession index and obliquity (Berger and Loutre, 1991). D: $^{40}Ar/^{39}Ar$ ages (2σ analytical error) of the Sulmona (central Apennine, Italy) tephras; F,G: $CaCO_3$ and oxygen isotope records from Sulmona lake sediments. H: δD in Antarctica European Project for Ice Coring in Antarctica (EPICA) Dome C ice record (Jouzel et al., 2007) on the Antarctic ice core chronology (AICC2012) age model (Bazin et al., 2013). I: Methane concentration in Dome C ice record (Loulergue et al., 2008) on the AICC2012 age model (Bazin et al., 2013). J,K: Ice rafted debris (IRD) and planktonic $\delta^{18}O$ records from North Atlantic Ocean Drilling Program (ODP) 983 based on its own astrochronological time scale (Kleiven et al., 2011).

Publisher: GSA
Journal: GEOL: Geology
DOI:10.1130/G36677.1

Figure 3. Synchronization of the Marine Isotope stage (MIS) 1 and MIS 19 palaeoclimatic records and orbital parameters. Each MIS 1 and MIS 19 time series was constructed on its own age model and aligned along the abrupt end of the Younger Dryas (YD) or YD-like event—as recorded in Alboran Sea and Sulmona records, respectively—which is assumed as time 'zero' of the relative time-scale. A–C: 21 June insolation at 65°N, precession index and obliquity (Berger and Loutre, 1991). D: Late Glacial-Holocene sea-surface temperature (SST) record from Alboran Sea (Martrat et al., 2014). E: Late MIS 20–MIS 19 oxygen isotope records from Sulmona (Italy) lake sediments. F: Methane concentrations in Late Glacial–Holocene, from Greenland North Greenland Ice Core Project (NGRIP) core (EPICA community members, 2006), and in late MIS 20–MIS 19, from Antarctica European Project for Ice Coring in Antarctica (EPICA) Dome C ice record (Loulergue et al., 2008), on the Antarctic ice core chronology (AICC2012) age model (Bazin et al., 2013). G: Carbon dioxide concentration in Late Glacial-Holocene (Monnin et al. 2004) and late MIS 20–MIS 19 (Bereiter et al., 2015) from the Antarctic Dome C core.

[1]GSA Data Repository item 2015xxx, additional information on $\delta^{18}O$, $\delta^{13}C$, $CaCO_3$, magnetic susceptibility, and $^{40}Ar/^{39}Ar$ analyses; detailed results of the $^{40}Ar/^{39}Ar$ dating for individual dated tephra; Figures DR1 and DR2; and full analytical details for individual crystals (Datasets DR1 and DR2), is available online at www.geosociety.org/pubs/ft2015.htm, or on request from editing@geosociety.org or Documents Secretary, GSA, P.O. Box 9140, Boulder, CO 80301, USA.

Publisher: GSA
Journal: GEOL: Geology
DOI:10.1130/G36677.1

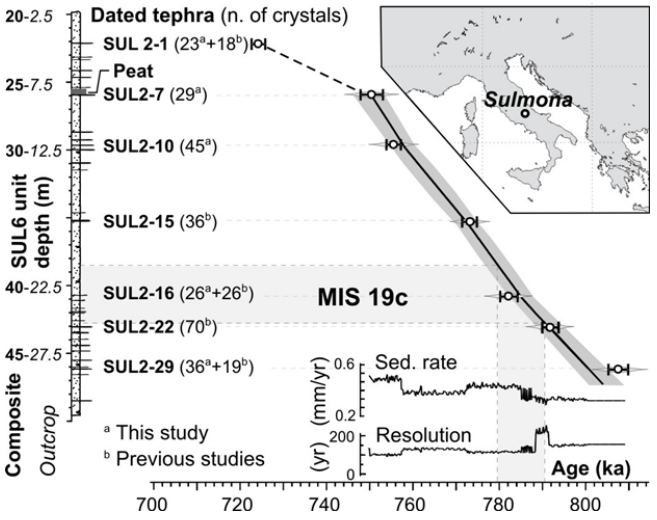

Figure 1

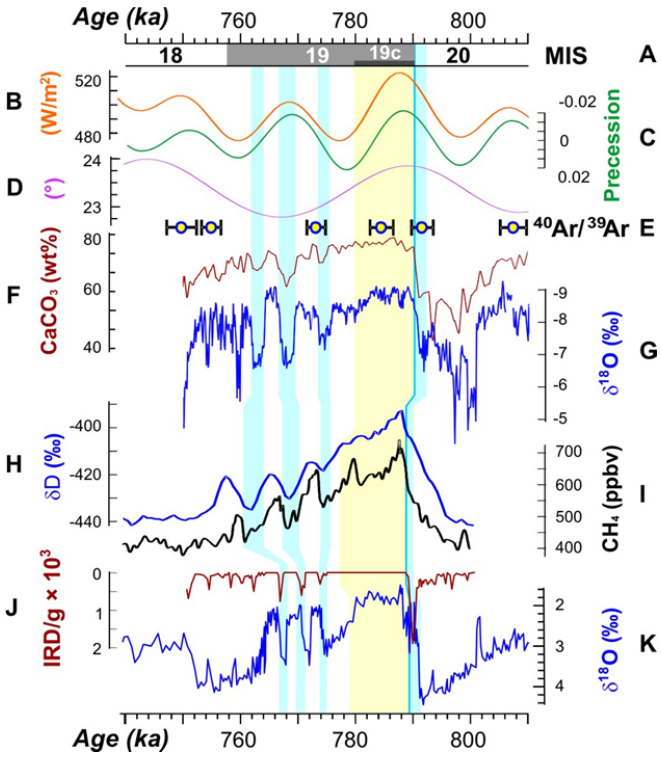

Figure 2

Publisher: GSA
Journal: GEOL: Geology
DOI:10.1130/G36677.1

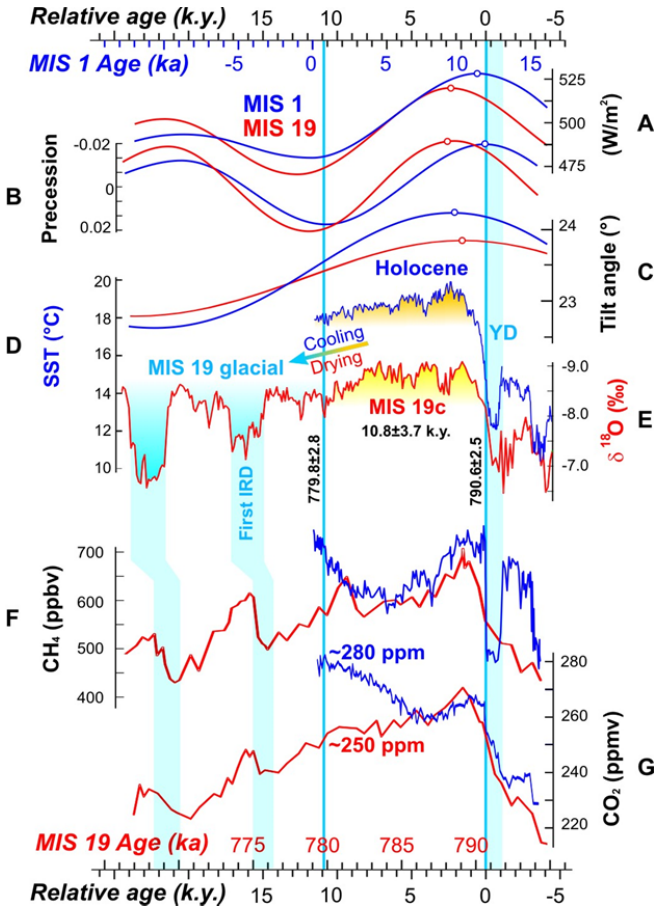

Figure 3

Publisher: GSA
Journal: GEOL: Geology
DOI:10.1130/G36677.1

DATA REPOSITORY: ADDITIONAL INFORMATION ON METHODS AND RESULTS

$\delta^{18}O$, $\delta^{13}C$, $CaCO_3$ and magnetic susceptibility analyses

The ca. 30 m-thick investigated interval (Fig. DR1) was sampled on the outcropping SUL6 succession with a resolution of ca. 5 cm. Samples were dried in an oven at 60 °C and carbonate content was obtained using gasometry on the bulk samples. A subsample of the dried samples was gently disaggregated and sieved at 100 μm to separate biogenic remains (e.g. ostracods and shells) from the sediments. The fraction below 100 μm was powdered and homogenized. To reduce any additional isotopic effect, no pre-treatment was performed before isotopic analyses following the recommendation of Wierzbowski (2007). Measurements were made using an Analytical Precision AP2003 continuous-flow isotope-ratio mass spectrometer (IRMS) at University of Melbourne, Australia. Samples were digested in 105% phosphoric acid at 70°C. Mass spectrometric measurements were made on the evolved CO_2. Results were normalized to the Vienna Pee Dee Belemnite scale using an internal working standard (NEW1 calibrated against the international standards NBS18 and NBS19). Mean analytical precision on internal standards is ± 0.10 and ± 0.05‰ for the AP2003. Internal reproducibility of the samples is ± 0.15‰.

Low field magnetic susceptibility was measured on whole SUL6 core section (d = 10 cm; Giaccio et al., 2013) every 10 cm with a Bartington MDR2 meter equipped with a MDR2C loop sensor.

$^{40}Ar/^{39}Ar$ dating of tephra layers

Pristine sanidine crystals from SUL2-1, SUL2-7, SUL2-10, SUL2-16 and SUL 2-29 tephra layers from SUL6 unit (Fig. 1) were handpicked under a binocular microscope and then slightly leached for 5 minutes in a 7 % HF acid solution in order to remove groundmass that could be still attached to them. Crystals at both Gif Laboratory and the Berkeley Geochronology Center (BGC) were picked from the same prepared sample for

Publisher: GSA
Journal: GEOL: Geology
DOI:10.1130/G36677.1
each respective tephra layer. Sample preparation was conducted at Gif laboratory. SUL2-7 was only analyzed at the BGC. SUL2-1, SUL2-16, SUL 2-29 $^{40}Ar/^{39}Ar$ results from Gif Laboratory were already published and discussed in Giaccio et al. (2013) and Sagnotti et al. (2014) and will therefore not be presented in more detail. A summary of both previous and new Gif, BGC, and final combined ages of the dated tephras is provided in Table DR1.

Gif analysis

About 40 crystals were handpicked after leaching and separately loaded in a single well in an aluminum disk and irradiated for 0.5 hours (IRR 50) in the β1 tube of the OSIRIS reactor (CEA Saclay, France). After irradiation, single crystals (300 to 400μm) were individually transferred into a stainless steel sample holder and then loaded into a differential vacuum Cleartran® window. Single crystals were fused at about 15 % of the full laser power using a 25 W CO_2 laser (Synrad®). Ar isotopes were analyzed using a VG5400 mass spectrometer equipped with a single ion counter (Balzers® SEV 217 SEN) following procedures outlined in Nomade et al. (2010). Each Ar isotope measurement consists of 20 cycles of peak switching of the argon isotopes. Neutron fluence (J) was monitored by co-irradiation of 1mm crystals of Alder Creek Sanidine (ACs-2, Nomade et al., 2005) placed in the same pit as the sample. J values were determined from analyses of three ACs-2 single grains for each sample. Procedural blanks were measured every three or four crystals (dataset DR2 in Data Repository). The precision and accuracy of the mass discrimination correction was monitored by daily measurements of air argon at various pressures (see full experimental description in Nomade et al., 2010). Nucleogenic production ratios used to correct for reactor produced Ar isotopes from K and Ca are given in the dataset DR2 and are from Nomade et al., (2014).

BGC analyses

Samples analyzed at the BGC were irradiated for 3 hours (IRR 423 PRA) and 0.5 hours (IRR 412 PRB) in the cadmium-lined CLICIT facility of the TRIGA reactor at Oregon State University. Neutron fluence was monitored by ACs standards bracketing the samples. J-values for each position were determined by the weighted mean of 5-6 analyses each comprising 3-5 grains of ACs. J-values for each of the samples were determined by a planar fit to the standard data.

Publisher: GSA
Journal: GEOL: Geology
DOI:10.1130/G36677.1
A MAP 215-50 mass spectrometer with a single analog electron multiplier was used. Data were acquired in 15 cycles of peak-hopping, and relative isotope abundances were determined by regression to an empirically determined equilibration time. Mass discrimination (1.01176 ±0.00106 per dalton) was corrected using the methods described in Renne et al. (2009), based on 37 air pipettes interspersed with the samples and standards. Procedural blanks were measured every 2-3 samples and standards, and their mean and standard deviation were applied for correction. Nucleogenic production ratios used to correct for reactor produced Ar isotopes from K and Ca are given in the dataset DR1.

$^{40}Ar/^{39}Ar$ Results

Detailed information on the $^{40}Ar/^{39}Ar$ dating for individual dated tephra are listed below and shown in Figure DR2 (for the age of the tephras SUL2-15 and SUL2-22 see Table DR1 and related references).

The reported ages are relative to the ACs age of 1.194 Ma (Nomade et al., 2010) and the decay constants of Steiger and Jäger (1977). Combined weighted mean ages and corresponding uncertainties are calculated using IsoPlot 3.0 (Ludwig, 2001) and are given at the 2σ level (analytical uncertainty).

SUL2-1: We combined the previously published results from Gif Sur Yvette Laboratory (Gif) (Giaccio et al., 2013) with the new data from the Berkley Geochronology Center (BCG) acquired in the present study (Table DR1; Fig. DR2). A total of 22 crystals were dated in Gif (Giaccio et al., 2013) and 29 in the BGC for this tephra layer. Ages obtained in the two labs are undistinguishable within uncertainty and were joined to obtain a combined weighted mean age of 724.4 ± 1.6 ka (MSWD = 0.9; P = 0.7) (Fig. DR2).

SUL2-7: A total of 31 crystals were dated at the BGC. Excluding two crystals obviously older, twenty nine crystals are used to calculate a weighted mean age of 749.4 ± 2.6 ka (MSWD = 0.7; P = 0.9) (Fig. DR2).

SUL2-10: 18 and 32 crystals were dated in Gif and the BGC respectively. The results from the two labs are indistinguishable at 95% confidence (Table DR1) and thus they were combined to obtain a weighted mean age of 755.1 ± 1.7 ka (MSWD = 1.2; P =

Publisher: GSA
Journal: GEOL: Geology
DOI:10.1130/G36677.1

0.13). Only five older crystals were rejected from the combined weighted mean calculation (Fig. DR2).

SUL2-16: 55 single crystal ages were obtained at the BGC. We combined these results with the data obtained in Gif and already published for the same tephra in Sagnotti et al. (2014) (Table DR1; Fig. DR2). In order to obtain a homogenous population of crystals that is statistically robust, we excluded 29 out of the 55 crystals measured at the BGC. These crystals are clearly statistically older and are the result of xenocrystic contamination. The higher proportion of xenocrysts in the BGC sample probably results from bias in selecting the grains to be analyzed at Gif, as it was the residue of this material that was sent to BGC. A combined weighted mean age based on 52 crystals analyzed in the two laboratories gives 782.2 ± 2.0 ka (MSWD = 0.6; P = 1.0) (Fig. DR2).

SUL2-29: We combined into a single dataset the 39 new $^{40}Ar/^{39}Ar$ single crystal ages obtained at the BGC with the ones already published (Sagnotti et al., 2014; Table DR1) on the same tephra layer. The combined weighted mean age is 807.8 ± 2.3 ka (MSWD = 0.8; P = 0.8) (Fig. DR2; Table DR1).

Table DR1: Gif, BGC and combined $^{40}Ar/^{39}Ar$ ages of the tephras from SUL6 Unit

Tephra	**Composite depth (m)**	**$^{40}Ar/^{39}Ar$ age (ka ± 2σ)**		
		Gif	**BGC**	**Combined**
SUL 2-1	22.2	724.1 ± 2.0[#]	725.4 ± 3.0*	724.4 ± 1.6
SUL 2-7	26.05		749.4 ± 2.6*	749.4 ± 2.6
SUL 2-10	29.07	754.9 ± 2.6*	760.4 ± 4.1*	755.1 ± 1.7
SUL 2-15	35.35	771.3 ± 2.0[§]	776.8 ± 2.7[§]	773.4 ± 1.6
SUL 2-16	40.8	781.3 ± 2.3[§]	783.0 ± 4.0*	782.2 ± 2.0
SUL 2-22	43.04	792.6 ± 2.5[§]	790.9 ± 2.8[§]	791.9 ± 1.9
SUL 2-29	46.14	810.4 ± 3.1[#, §]	804.0 ± 3.4*	807.8 ± 2.3

* This study; [#] Giaccio et al., 2013; [§] Sagnotti et al., 2014.

Publisher: GSA
Journal: GEOL: Geology
DOI:10.1130/G36677.1

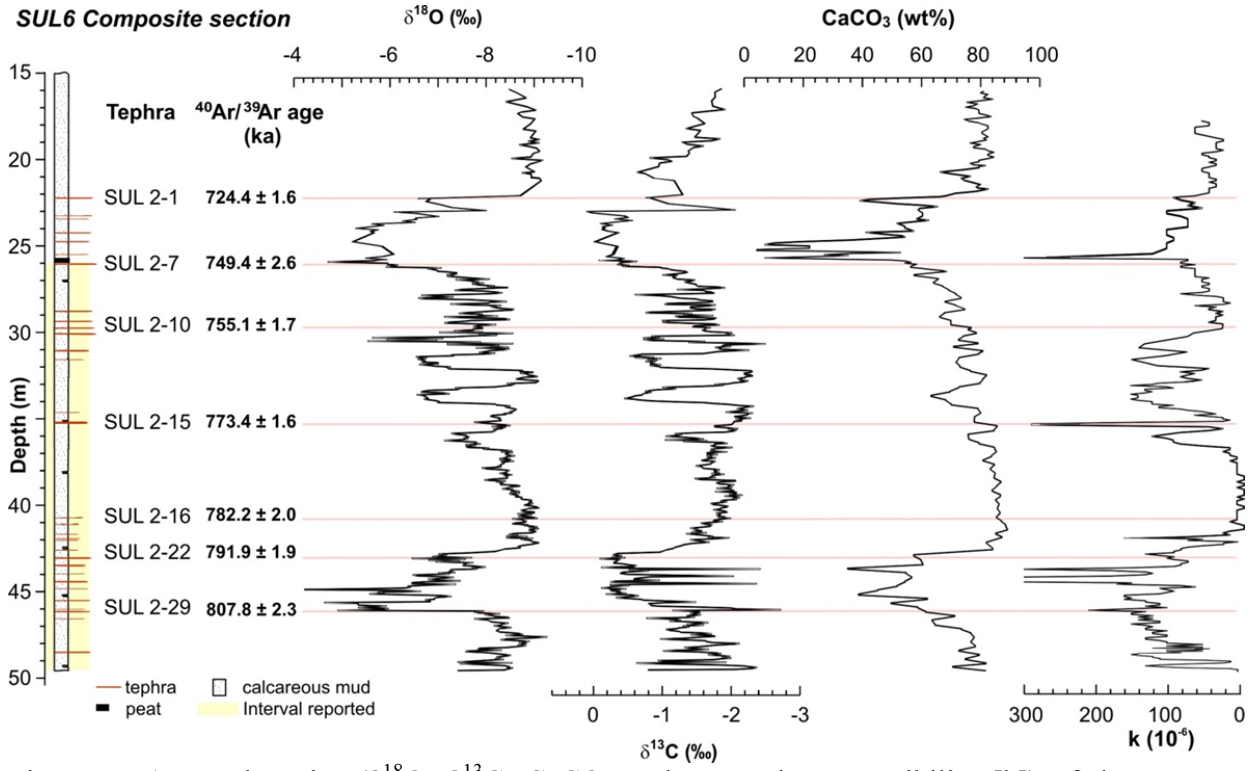

Figure DR1. Depth series ($\delta^{18}O$, $\delta^{13}C$, $CaCO_3$ and magnetic susceptibility [k]) of the investigated Sulmona 6 (SUL6) unit. The yellowish bar, between the depths of ca. 26 m and ca. 49.5 m, represents the stratigraphic interval presented in this study. The position and the ages of the seven $^{40}Ar/^{39}Ar$ dated tephras (pink lines) are also shown.

Publisher: GSA
Journal: GEOL: Geology
DOI:10.1130/G36677.1

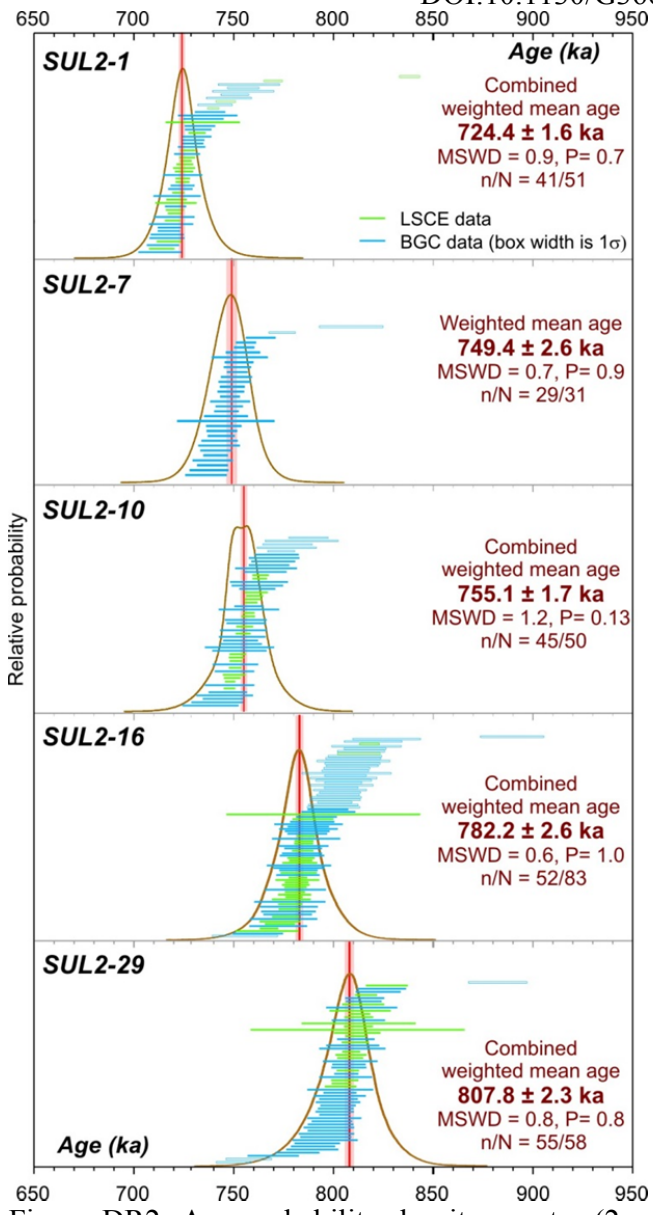

Figure DR2. Age-probability density spectra (2σ analytical uncertainty) and individual crystal age for SUL2-1, SUL2-7, SUL2-10, SUL2-16 and SUL2-29 tephra layers (for the age of the tephras SUL2-15 and SUL2-22 see Table DR1 and related references). Blue and green boxes (1σ) are individual crystals analyzed at the Berkeley Geochronology Center (BGC) and Gif Sur Yvette (LSCE), respectively. Blank boxes are the excluded crystals.

Publisher: GSA
Journal: GEOL: Geology
DOI:10.1130/G36677.1

Age Model Parameters

The Bacon age-depth model employed the following parameters: acc.shape = 1.5; acc.mean = 20; mem.strength = 1; mem.mean = 0.1; 121 20cm sections.

REFERENCES CITED

Giaccio, B., Castorina, F., Nomade, S., Scardia, G., Voltaggio, M., and Sagnotti, L., 2013, Revised chronology of the Sulmona lacustrine succession, central Italy; Journal of Quaternary Science, v. 28, p. 545–55.

Ludwig, K.R., 2001. Isoplot 3-A Geochronological Toolkit for Microsoft Excel. Special Publication No 4 Berkeley Geochronology Center (Berkeley), 71 p.

Nomade, S., Gauthier, A., Guillou, H., and Pastre, J.F., 2010, 40Ar/39Ar temporal framework for the Alleret maar lacustrine sequence (French Massif-Central): Volcanological and paleoclimatic implications: Quaternary Geochronology, v. 5, 20–27.

Nomade, S. Pastre, J.F., Guillou H., Faure, M., Guérin, G., Delson, E., Debard, E., Voinchet, P., and Messager. E., 2014, $^{40}Ar/^{39}Ar$ constraints on some French landmark Late Pliocene to Early Pleistocene large mammalian paleofauna: paleoenvironmental and paleoecological implications: Quaternary Geochronology, v. 21, p. 2–15.

Nomade S., Renne, P.R., Vogel, N., Deino A.L., Sharp. W.D., Becker, T.A., Jaouni, A.R., and Mundil, R., 2005, Alder Creek Sanidine (ACs-2): A Quaternary $^{40}Ar/^{39}Ar$ standard: Chemical Geology, v. 218 (3/4), p 319–342.

Renne, P.R., Cassata, W.S., and Morgan, L.E., 2009, The isotopic composition of atmospheric argon and $^{40}Ar/^{39}Ar$ geochronology: time for a change?: Quaternary Geochronology, v. 4, p. 288–298.

Sagnotti, L., Scardia, G., Giaccio, B., Liddicoat, J.C., Nomade, S., Renne, P.R., and Sprain, C.J., 2014, Extremely rapid directional change during Matuyama-Brunhes geomagnetic polarity reversal: Geophysical Journal International, v. 199, p. 1110–1124.

Publisher: GSA
Journal: GEOL: Geology
DOI:10.1130/G36677.1
Steiger, R.H., and Jäger, E., 1977, Subcommission on geochronology: convention on the use of decay constants in geo- and cosmochronology: Earth. Planet. Sci. Lett., v. 36, p. 359–362.

Wierzbowski, H., 2007, Effects of pre-treatments and organic matter on oxygen and carbon isotope analyses of skeletal and inorganic calcium carbonate: International Journal of Mass Spectrometry, v. 268, p. 16–29.